Journal of Innate Immunity

Research Article

J Innate Immun 2022;14:673–689
DOI: 10.1159/000523991

Received: November 24, 2021
Accepted: February 21, 2022
Published online: April 20, 2022

GDF15 Suppresses Lymphoproliferation and Humoral Autoimmunity in a Murine Model of Systemic Lupus Erythematosus

Georg Lorenz[a, b] Andrea Ribeiro[a, c] Ekatharina von Rauchhaupt[a] Vivian Würf[a] Christoph Schmaderer[c] Clemens D. Cohen[a] Twinkle Vohra[d] Hans-Joachim Anders[a] Maja Lindenmeyer[e] Maciej Lech[a]

[a]LMU Klinikum, Medizinische Klinik und Poliklinik IV, Department of Nephrology, Ludwig-Maximilians-Universität München, Munich, Germany; [b]Klinikum rechts der Isar, Department of Nephrology, Section of Rheumatology, Technical University Munich, Munich, Germany; [c]Klinikum rechts der Isar, Department of Nephrology, Technical University Munich, Munich, Germany; [d]LMU Klinikum, Medizinische Klinik und Poliklinik IV, Department of Endocrinology, Ludwig-Maximilians-Universität München, Munich, Germany; [e]III. Department of Medicine, University Medical Center Hamburg-Eppendorf, Hamburg, Germany

Keywords
Autoimmunity · Lupus nephritis · Growth and differentiation factor 15 · Autoantibodies · Toll-like-receptor · Macrophages · Inflammation

Abstract
Growth and differentiation factor 15 (GDF15), a divergent member of the transforming growth factor-β superfamily, has been associated with acute and chronic inflammatory conditions including autoimmune disease, i.e., type I diabetes and rheumatoid arthritis. Still, its role in systemic autoimmune disease remains elusive. Thus, we studied GDF15-deficient animals in Fas-receptor intact (C57BL/6) or deficient (C57BL/6$^{lpr/lpr}$) backgrounds. Further, lupus nephritis (LN) microdissected kidney biopsy specimens were analyzed to assess the involvement of GDF15 in human disease. GDF15-deficiency in lupus-prone mice promoted lymphoproliferation, T-, B- and plasma cell-expansion, a type I interferon signature, and increased serum levels of anti-DNA autoantibodies. Accelerated systemic inflammation was found in association with a relatively mild renal phenotype. Splenocytes of phenotypically overall-normal *Gdf15–/–* C57BL/6 and lupus-prone C57BL/6$^{lpr/lpr}$ mice displayed increased in vitro lymphoproliferative responses or interferon-dependent transcription factor induction in response to the toll-like-receptor (TLR)-9 ligand CpG, or the TLR-7 ligand Imiquimod, respectively. In human LN, GDF15 expression was downregulated whereas type I interferon expression was upregulated in glomerular- and tubular-compartments versus living donor controls. These findings demonstrate that GDF15 regulates lupus-like autoimmunity by suppressing lymphocyte-proliferation and -activation. Further, the data indicate a negative regulatory role for GDF15 on TLR-7 and -9 driven type I interferon signaling in effector cells of the innate immune system.

Introduction

Systemic lupus erythematosus (SLE) is a classic example of systemic autoimmunity. Genetic susceptibility, female sex-specific factors, and environmental triggers,

Karger@karger.com
www.karger.com/jin

Correspondence to:
Maciej Lech, maciej.lech@med.uni-muenchen.de

e.g., viral infections are key determinants of SLE onset. In established disease, a misguided "self-directed" adaptive immune response provokes autoantibody production and lymphadenopathy. Furthermore, erroneous recognition of nucleic acids, e.g., by toll-like receptors (TLRs) and the subsequent type I interferons secretion by dendritic cells and macrophages confirm an essential role of innate immunity in the pathogenesis of SLE [1]. Both systems are involved in organ damage resulting from autoimmunity. For instance, in lupus nephritis (LN) immune complex deposition induces local immune cell activation and increases immune cell influx leading to tissue damage [1, 2].

Growth differentiation factor 15 (GDF15), originally discovered as macrophage inhibitory cytokine 1 (MIC1), is a cytokine belonging to the transforming growth factor (TGF-β) superfamily [3, 4]. Although the members of this family are structurally related, they are quite divergent from each other regarding their amino acid sequences and their specific activities in vitro and in vivo [5]. GDF15 shares only 30% sequence homology with other family members such as TGF-β1 suggesting a nonredundant biologic activity [3, 6]. Nevertheless, the latter is well known for its immune-regulatory functions. Moreover, TGF-β1 deficiency leads to a lethal autoinflammatory disorder with some autoimmune features in mice [7, 8].

The constitutive expression of GDF15 is restricted to reproductive organs whereas other cell types, e.g., macrophages, show inducible expression upon tissue injury or pro-inflammatory, stress-induced factors such as TNFα [9]. For instance, in LPS-induced murine sepsis, GDF15 improved survival by stimulating hepatic triglyceride metabolism to promote tissue tolerance against inflammatory damage [10]. Studies by Kempf et al. [11] have demonstrated the anti-apoptotic function of GDF15 in response to heart ischemia and myocardial infarction. More recently, their studies proved that the lack of GDF15 upturns the infiltration of polymorphonuclear leukocytes into the site of inflammation. Consequently, GDF15 reduces leukocyte recruitment by abating chemokine signaling [12]. Our recent study suggests the modulation of the CXCR3 receptor in activated T-cells as a possible GDF15-dependent mechanism that regulates the infiltration of T cells in anti-GBM nephritis in mice [13].

How GDF15 modulates immune-cell signaling is not clear yet. Expression of its known receptor GDNF family receptor alpha-like (GFRAL) is restricted to cerebral tissues and additional signaling pathways seem mandatory [9]. Most recently, an immunosuppressive effect via CD48/STUB1 signaling in Tregs has been reported in a hepatocellular carcinoma transgenic mouse model [14]. In accordance, others found the GDF15 to stimulate Treg maturation with a significant correlation between FoxP3 and GDF15 expression [15]. GDF15 was reported to suppress dendritic cells (DCs) maturation, DC-MHCII-expression, and IL-12 secretion in tumor-bearing mice [16]. GDF15 was also shown to act as a paracrine factor, required for M2-like macrophage polarization, reversal of inflammatory adipose tissue inflammation and insulin resistance in mice [17]. Cumulatively, these data indicate that the immune regulatory role of GDF15 goes beyond acute inflammation and tissue injury. GDF15 might impact chronic inflammation and autoimmunity. In fact, GDF15 serum levels were shown to be positively correlated with disease activity in rheumatoid arthritis patients [9, 18]. In addition, proteomic analysis has shown an absence of GDF15 in islet cells from individuals with an inflammatory stage of type I diabetes [19]. Likewise, LN patients from a decent-sized cohort showed elevated serum GDF15 levels. Although only a mild association ($r = 0.23$, $p = 0.03$) of GDF15 with SLEDAI-2K clinical activity scoring was reported, the authors found a strong univariate association of serum GDF15 with creatinine levels ($r = 0.71$, $p < 0.001$) and proteinuria ($r = 0.56$, $p < 0.01$) [20].

Considering (a) the ability of GDF15 to stimulate immunoregulatory Treg maturation as well as their role in immune tolerance [21] and (b) the pleiotropic suppressive function of GDF15 on DC and macrophage activation and their role in systemic inflammation [22], we hypothesized that GDF15 suppresses progression of lupus-like autoimmunity in mice. In particular, we postulated an aggravated serologic and nephritic phenotype in lupus-prone C57BL/6$^{lpr/lpr}$ mice in the absence of GDF15.

Materials and Methods

Animal Studies

Mouse colonies were generated by backcrossing the *Gdf15*−/− strain (MGI: 2386300, *Gdf*15^{tm1Sjl}) [23] into C57BL/6J parental strain obtained from Jackson Laboratories for at least 6 generations. Later *Gdf15*−/−$^{lpr/lpr}$ mice were generated by crossing *Gdf15*−/− and C57BL/6$^{lpr/lpr}$ (B6.MRL-Faslpr/J, Stock No: 000482 obtained from Jackson Laboratories) for four generations. Newly established colonies of wild-type and mutant mice in the C57BL/6 background (parental strain C57BL/6J) were used for experiments. The *Gdf15*−/−$^{lpr/lpr}$ mice were born at Mendelian ratios and display common litter sizes. The genotype was assured by PCR. Mice were housed in groups of 5 mice in sterile filter top cages with a 12 h dark/light cycle and unlimited access to autoclaved food and water. We used only female mice for all experiments. All mice were sacrificed by cervical dislocation at 24 weeks of age. This study was

Table 1. Primer sequences for the quantitative PCR

Gene name	Accession No.	Forward primer	Reverse primer
Casp3	NM_001284409	5′-TGCTGGTGGGATCAAAGC-3′	5′-TGAATCCACTGAGGTTTTGTTG-3′
Cd 40	NM_011611	5′-ACCAGCAAGGATTGCGAGGCAT-3′	5′-GGATGACAGACGGTATCAGTGG-3′
Cd 40l	NM_011616	5′-GAACTGTGAGGAGATGAGAAGGC-3′	5′-TGGCTTCGCTTACAACGTGTGC-3′
Cxcl 13	NM_018866	5′-CATAGATCGGATTCAAGTTACGCC-3′	5′-GTAACCATTTGGCACGAGGATTC-3′
Dhx 9	NM_007842	5′-GGCAATCGAACCTCCACCTTTG-3′	5′-GGAGTTTAGCCAGGATTCGTCC-3′
Dhx 36	NM_028136	5′-GTCTTTCTACCAGGCTGGGACA-3′	5′-GTGTCTGGTTGACGGTAGGCAT-3′
Dnase 1	NM_010061	5′-CTGAGTCGCTATGACATCGCTG-3′	5′-CTACATAGCGGTAGGTGTCAGG-3′
Flt3l	NM_010228	5′-TGGATGAGCAGTGTGAACCGCT-3′	5′-GCCAAATGCAGAGGCTTGAACG-3′
GAPDH	NM_001289726	5′-CATGGCCTTCCGTGTTCCTA-3′	5′-CCTGCTTCACCACCTTCTCA-3′
GM-CSF	NM_009969	5′-CGGCCTTGGAAGCATGTAGA-3′	5′-CACAGTCCGTTTCCGGAGTT-3′
Ifi204	NM_008329	5′-CCAGTCACCAATACTCCACAGC-3′	5′-CTCTGAGTGGAGAACAGCACCT-3′
Ifit1	NM_008331	5′-CAAGGCAGGTTTCTGAGGAG-3′	5′-GACCTGGTCACCATCAGCAT-3′
Ifit3	NM_010501	5′-TTCCCAGCAGCACAGAAAC-3′	5′-AAATTCCAGGTGAAATGGCA-3′
Ifnα4	NM_010504	5′-TTCTGCAATGACCTCCATCA-3′	5′-TATGTCCTCACAGCCAGCAG-3′
Ifnα6	NM_206,871	5′-TGGAATGCAACCCTCCTAGA-3′	5′-TCAGGGGAAGTGCCTGTATC-3′
Ifnβ	NM_010510	5′-CTCAGGGTGTCGATGAGGTC-3′	5′-CCCAGTGCTGGAGAAATTGT-3′
Infλ2	NM_001024673	5′-CCAGTGGAAGCAAAGGATTGCC-3′	5′-TCAGGTCCTTCTCAAGCAGCCT-3′
Ifnλ3	NM_177,396	5′-CCAGTGGAAGCAAAGGATTGCC-3′	5′-GCACCTCATGTCCTTCTCAAGC-3′
Il-2	NM_008366	5′-GCGGCATGTTCTGGATTTGACTC-3′	5′-CCACCACAGTTGCTGACTCATC-3′
Il-4	NM_021283	5′-ATGGATGTGCCAAACGTCCT-3′	5′-AGCTTATCGATGAATCCAGGCA-3′
Il-5	NM_010558	5′-GATGAGGCTTCCTGTCCCTACT-3′	5′-TGACAGGTTTTGGAATAGCATTTCC-3′
Il-7	NM_008371	5′-CAGGAACTGATAGTAATTGCCCG-3′	5′-CTTCAACTTGCGAGCAGCACGA-3′
Il-9	NM_008373	5′-TCCACCGTCAAAATGCAGCTGC-3′	5′-CCGATGGAAAACAGGCAAGAGTC-3′
Il-10	NM_010548	5′-ATCGATTTCTCCCCTGTGAA-3′	5′-TGTCAAATTCATTCATGGCCT-3′
Il-12	NM_001159424	5′-CTAGACAAGGGCATGCTGGT-3′	5′-GCTTCTCCCACAGGAGGTTT-3′
Il-15	NM_001254747	5′-GTAGGTCTCCCTAAAACAGAGGC-3′	5′-TCCAGGAGAAAGCAGTTCATTGC-3′
Il-23	NM_031252	5′-CATGCTAGCCTGGAACGCACAT-3′	5′-ACTGGCTGTTGTCCTTGAGTCC-3′
Mavs	NM_001206382	5′-CTGCCAACACAATACCACCTGAG-3′	5′-TCTCTGGTCCAGAGTGCAAGCT-3′
Mx1	NR_003520	5′-TCTGAGGAGAGCCAGACGAT-3′	5′-CTCAGGGTGTCGATGAGGTC-3′
Prdm1	NM_007548	5′-ACCAAGGAACCTGCTTTTCA-3′	5′-TAGACTTCACCGATGAGGGG-3′
Tgfβ	NM_011577	5′-GGAGAGCCCTGGATACCAAC-3′	5′-CAACCCAGGTCCTTCCTAAA-3′
Tlr7	NM_001290755	5′-GGATGATCCTGGCCTATCTC-3′	5′-TGTCTCTTCCGTGTCCACAT-3′
Tlr9	NM_031178	5′-CAGTTTGTCAGAGGGAGCCT-3′	5′-CTGTACCAGGAGGGACAAGG-3′
TNF	NM_013693	5′-GATCGGTCCCCAAAGGGATG-3′	5′-GGTGGTTTGCTACGACGTG-3′
Tnfsf 13	NM_001159505	5′-GTTGCTCTTTGGTTGAGTTGGG-3′	5′-GTTGGATCAGTAGTGCGACAGC-3′
Tnfsf 13b	NM_033622	5′-CCTCCAAGGCATTTCCTCTT-3′	5′-GACTGTCTGCAGCTGATTGC-3′
Zbp1	NM_021394	5′-GATCTACCACTCACGTCAGGAAG-3′	5′-GGCAATGGAGATGTGGCTGTTG-3′

carried out following the principles of the Directive 2010/63/EU on the Protection of Animals Used for Scientific Purpose and with approval by the local government authorities.

Evaluation of Autoimmune Tissue Injury

Organs (spleens and kidneys) from female mice were fixed in 4% buffered formalin, processed, and embedded in paraffin. The severity of the renal lesions was graded on periodic acid-Schiff (PAS) stained sections using the indices for activity and chronicity. Histology stainings were performed following the manufacturer's instructions. We used following antibodies: rat Blimp1 (cat. 14-5963-82, Invitrogen, 1:100); rat B220 (cat. 14-0452-82, Invitrogen, 1:400); Ki67 (Bio-Rad, 1:100); Mac2 (125402 BioLegend, 1:3000); CD45 (cat. 5188647, BD, 1:100); C9 (PA5-29093, Invitrogen, 1:50); WT-1 (MA5-32215, Invitrogen, 1:100). For quantitative analysis, glomerular cells were counted in 10 cortical glomeruli per section (from "*n*" mice in the group, as indicated in a figure) or were analyzed using Adobe Photoshop CS4Extended (Adobe, San Jose, CA, USA) (% of stained high power field). The kidney function of 6-month-old female mice from every group was determined by measuring serum creatinine levels determined by the Jaffe method (DiaSys Diagnostic Systems). Albuminuria and proteinuria were determined via mouse Albumin Quantification Set (Bethyl Laboratories, Montgomery, TX, USA) and Bradford method, respectively. Urinary albumin excretion was evaluated by a double-sandwich ELISA. First, 96-well plates were coated with goat anti-mouse albumin antibody A90-13A-5 (Bethyl Laboratories, Montgomery, TX, USA), and plates were incubated overnight at 4°C. After blocking for half an hour at room temperature in 0.5% BSA in PBS with 0.05% Tween20, urine samples, and mouse albumin standard (Sig-

ma-Aldrich, St. Louis, MI, USA) were added on the plate in triplicates for 2 h. Mouse urine samples were diluted in serial dilutions ranging from $1:10^2$ to $1:10^7$. As a secondary antibody, HRP-conjugated anti-mouse albumin antibody A90-134P-7 (Bethyl Laboratories) was used.

Flow Cytometry

Compensation was done using the following antibodies on pooled mice splenocytes. Before gating doublets were excluded on FSC-(H)ight versus FSC-(W)idth blots. After compensation using the following antibodies on pooled mice splenocytes, splenic T cells were identified using anti-mouse CD3 FITC (#553062 BD), CD4 APC (#553051 BD), CD8a PerCP (#553030 BD), and CD44 P3 (#553134 BD). PI was used for dead cell exclusion. Tregs were identified using the BD Th17/Treg mouse phenotyping kit following the manufacturer's instructions (#560767 BD). B cells were stained using anti-mouse FITC MHC II (11532185 eBioscience), B220 Alexa Fluor 647 (clone RA3-6B2 BioLegend) and CD19 PB450 (clone 6D5, BioLegend). PI was used for the exclusion of dead cells. Plasma cells were stained intracellularly with anti-mouse kappa light chain PE (#559940, BD). In addition, anti-mouse CD138 APC (#558626, BD) and anti-mouse FITC MHC II (#11532185 eBioscience) were used. Zombie NIR™ fixable viability dye (#423106 BioLegend) was used for dead cell exclusion. Splenic macrophages and dendritic cells were analysed after staining for anti-mouse CD86 FITC (#553691 BD), CD11c PE (#557401, BD), F4/80 APC (clone MCA497 BioRad/AbDSeroTec). PI was used for dead cell exclusion. Plasmacytoid dendritic cells (pDCs) were identified using CD11c PE (#557401, BD), B220 Alexa Fluor 647 (clone RA3-6B2 BioLegend), and anti-mouse CD317 PE (# 127104, BioLegend). Intracellular labeling was done using the Cytofix/Cytoperm kit (BD), following the manufacturer's instructions. Cell counting beads (Invitrogen) were used for determining cell numbers by FACS Cytoflex (Beckman Coulter, Indianapolis, IN, USA) and analyzed with FlowJo V.10 Software (BD). The gating strategy is presented in online supplementary Figure 4 (see www.karger.com/doi/10.1159/000523991 for all online suppl. material).

Real-Time Quantitative PCR

Real-time RT-PCR was performed on total spleen mRNA and whole blood samples as well as in vitro experiments. Shortly SYBR Green Dye detection system was used for quantitative real-time PCR on Light Cycler 480 (Roche, Mannheim, Germany). Gene-specific primers (225 nM, Metabion, Martinsried, Germany) were used as listed in Table 1. Controls consisting of ddH2O were negative for target and housekeeper genes. Gapdh mRNA was used as a housekeeper. The PCRs were performed in 96-well plates according to the manufacturer protocol (Light Cycler 480 II). Standard controls on each array for genomic DNA contamination, RNA quality, and general PCR performance were included.

Autoantibody and Plasma Analysis

For detection of antibodies to double-stranded DNA, NUNC MaxiSorp ELISA plates (Thermo Fisher Scientific) were coated with poly-L-lysine (Trevigen) and PBS (ratio 1:1) for 1 h. Plates were washed with TrisNaCl (50 mM Tris and 0.14 M NaCl pH 7.5) and double-stranded DNA (2 μg/mL) was coated in SSC pH 7.0 buffer overnight. For anti-Smith and anti-histone antibodies, MaxiSorp ELISA plates were coated with Smith antigen (Sm3000; Immunovision) or histones (2 μg/mL) in 0.05 M carbonate-bicarbonate buffer overnight at 4°C. Serum samples were diluted 1:100–1:1.000.000 for all IgM/IgG ELISAs. Sera from 24-week C57BL/6, C57BL/$6^{lpr/lpr}$, 24-week MRL$^{lpr/lpr}$ mice were used as controls. Horseradish peroxidase-conjugated antibody to mouse IgG and IgM (A90-131P and A90-101A, Bethyl) was used as a secondary antibody (1:50.000). Absorbance was measured at 450 nm with a Sun-rise plate reader (TECAN). BD Cytometric Bead Array (CBA) Mouse Inflammation Kit as well as standard BD and R&D ELISAs (Mouse Quantikine ELISA Kits) were used to determine the pro-inflammatory cytokines according to manufacturer protocol. For cytokine analysis of serum from mice or cell culture experiments, samples were prepared according to the instruction of the BD Cytometric Bead Array Mouse Inflammation Kit. The concentrations of the cytokines IL-6, IL-10, MCP-1, IFN-γ, TNF, and IL-12p70 in the samples were determined by the software FCAP software V2. Plasma aldosterone levels were analysed using an enzyme-linked immunosorbent assay (ELISA, RE52301, IBL International GmbH, Hamburg, Germany). Briefly, the plasma samples were diluted (1:5) with deionized water and loaded into the microtiter wells coated with polyclonal rabbit antibodies directed against the antigenic site of the aldosterone molecule. All consequent steps were performed as per the manufacturer`s protocol. The absorbance (OD) of each well was measured at 450 ± 10 nm using a microtiter plate reader (FLUOstar Omega, Serial no. 415-2731, BMG Labtech, Ortenberg, Germany). Plasma corticosterone levels were measured using a high sensitivity enzyme immunoassay (EIA, AC-15F1, Immunodiagnostic Systems Limited, United Kingdom) as per the manufacturer's protocol. Briefly, the plasma samples were diluted with the provided diluent in the ratio of 1:50 and heated at 80°C for 10 min. The samples were then incubated with horseradish peroxidase (HRP)-conjugated polyclonal corticosterone antibody in the microtiter wells for 4 h at room temperature. The wells were washed and TMB (3,3′,5,5′-Tetramethylbenzidine, chromogenic substrate) was added. The generated color was measured at the absorbance of 450 nm in a microplate plate reader (FLUOstar Omega, Serial no. 415-2731, BMG Labtech, Ortenberg, Germany). The amount of extracellular DNA in serum was quantified using Quant-iT PicoGreen dsDNA Reagent (QPG; Invitrogen/ThermoFisher Scientific). QPG was diluted 1:200 in TE buffer (10 mM Tris, 1 mM EDTA [pH 7.5]), and 90 μL was mixed with 10 μL of serum (dilution 1:2–1:50) containing extracellular DNA. The fluorescence was measured at an excitation wavelength of 480 nm and an emission wavelength of 520 nm. We used the information about numbers of long interspersed nuclear element-1 (LINE-1 or L1) elements in mammalian genomes to prepare the standard curve [24]; 1 μg of mouse genomic DNA corresponds to 3.4×105 copies of a single-copy gene. We used following primers to estimate the cell-free DNA in 2 μL (1:10 diluted) serum (mitochondrial DNA Fw: GCCCATGACCAACATAACTG, Rv: CCTTGACGGCTATGTTGATG; Line element Fw: ACCAAATGGCTGAGAAGCAC, Rv: ATCTGCTGTCGCCTGAATTT).

In vitro Experiments

Splenocytes cells from wild-type and knockout mice were isolated from fresh spleens, erythrocyte-depleted, and cultured in DMEM medium supplemented with 2% FCS and 1% penicillin/streptomycin for 48 h. Bone marrow cells from wild-type and knockout mice were isolated from femur and tibia, erythrocyte-depleted, and cultured with 20 ng/mL mouse recombinant M-CSF

(Immunotools, Friesoythe, Germany) in DMEM medium supplemented with 10% FCS and 1% penicillin/streptomycin for 7 days to generate macrophages. Bone marrow cells from wild-type and knockout mice were isolated from femur and tibia, erythrocyte-depleted, and cultured with 20 ng/mL mouse recombinant GM-CSF or Flt3L (Immunotools, Friesoythe, Germany) in DMEM medium supplemented with 10% FCS and 1% penicillin/streptomycin for 7 days to generate cDCs and pDCs, respectively. On day 7, cells were stimulated with 10 ng/mL LPS, 100 ng/mL ODN 1668 B-class CpG specific for mouse TLR-9, 1 μg/mL Imiquimod, 100 ng of Poly(I:C), 20 ng/mL IFNγ, or left untreated as media control. All ligands and cytokines were obtained from Invivogen. After 4 h, macrophages were lysed and processed for gene expression analysis (qRT-PCR). The cytokines in the supernatants were determined after 24 h. Cell viability and metabolic activity were assessed by MTT (3-(4,5-dimethylthiazol-2-yl)-2,5-diphenyltetrazolium bromide) assay accordingly to manufacturer instruction (Sigma-Aldrich). We used 50 ng/mL ODN 1668 B-class CpG specific for mouse TLR-9. Mouse splenocytes from WT and knockout mice were assessed by MTT assay up to 72 h in medium supplemented with 2% FCS; 10% FCS was used as an additional control.

Human Array Data

Human kidney biopsy specimens and Affymetrix microarray expression data were procured within the framework of the European Renal cDNA Bank-Kröner-Fresenius Biopsy Bank. Biopsies were obtained from patients after informed consent and with the approval of the local Ethics Committees [25]. Biopsies were processed as previously reported [26]. Published gene expression profiles (Affymetrix GeneChip Human Genome U133A and U133 Plus2.0 Arrays; GSE99340, GSE32591, GSE35489, GSE37463) used in this study came from patients with HTN(Glom: n = 15; Tub: n = 21), minimal change disease (MCD; Glom: n = 14; Tub: n = 15), and LN (Glom: n = 32; Tub: n = 32). Pretransplantation kidney biopsies from living donors (LD, Glom: n = 42, Tub: n = 42) were used as control renal tissue. CEL file normalization was performed with the Robust Multichip Average method using RMAExpress (Version 1.0.5) and the human Entrez-Gene custom CDF annotation from Brain Array version 18 (http://brainarray.mbni.med.umich.edu/Brainarray/Database/CustomCDF/CDF_download.asp).

The log-transformed dataset was corrected for batch effect using ComBat from the GenePattern pipeline (http://www.broadinstitute.org/cancer/software/genepattern/). To identify differentially expressed genes, the Significance Analysis of Microarrays (SAM) method was applied using TiGR (MeV, Version 4.8.1) [27]. Tubulointerstitial and glomerular gene expression profiles from patients with different chronic kidney diseases (MCD, HTN, LN) and controls (LD) were used to compute the correlation of the log-transformed steady-state expression levels of GF15 with Type-I interferon- and Ki-67 gene expression using Spearman correlation (GraphPad Prism 8.0).

Statistical Analysis

Data were expressed as mean ± SEM to take into account both the value of the SD and the sample size instead of variability among replicates. The one-way analysis of variance (ANOVA) was used to determine statistics in the case of three or more independent (unrelated) groups. Tukey's multiple comparison test was used for all-possible pairwise comparisons. The student's t test was used for direct comparisons between single groups, i.e., wild type and knockout cells/mice in case of normally distributed data or sample size $n > 15$. Mann-Whitney U test was used to analyze data with small sample size and nonparametric distribution of data. We used GraphPad Prism software. Statistical significance was indicated as follows: p value of <0.05 (*); p value of <0.01 (**); p value of <0.001 (***).

Results

GDF15 Suppresses Lymphocyte Proliferation in Murine Lupus-Like Disease

First, we evaluated female GDF15-deficient mice for signs of spontaneous autoimmunity. We did not observe any significant differences between *Gdf15*–/– and wild-type C57BL/6 mice in body weight (Fig. 1a). Up to 6 months of age *Gdf15*–/– mice did not display lymphoproliferation, splenomegaly, or autoantibodies in serum (Fig. 1b, c; the level of antibodies will be discussed later in the results chapter and Fig. 3). Simultaneously, we generated GDF15-deficient C57BL/6$^{lpr/lpr}$ mice by crossing *Gdf15*–/– mice with autoimmune-prone C57BL/6$^{lpr/lpr}$ mice deficient for the *Fas*-receptor (CD95) as described in materials and methods. GDF15 serum levels of 6-months old mice were comparable in both C57BL/6 and autoimmune C57BL/6$^{lpr/lpr}$ background (Fig. 1d). Despite similar body weights (Fig. 1a), *Gdf15*–/–$^{lpr/lpr}$ mice displayed significant lymphadenopathy and splenomegaly compared with C57BL/6$^{lpr/lpr}$ controls (Fig. 1b, c). Splenic Ki-67 staining revealed increased lymphocyte proliferation (Fig. 1e). *Gdf15*–/–$^{lpr/lpr}$ mice also showed increased splenic mRNA expression of *DNAse-I* and *Caspase-3* and increased absolute numbers of late apoptotic/necrotic (PI+) splenocytes, cumulatively indicating an increased "cellular turnover" and possibly nucleic acid exposure (Fig. 1f–h). In fact, sera from *Gdf15*–/–$^{lpr/lpr}$ but not *Gdf15*–/– mice contained increased concentrations of cell-free DNA (Fig. 1i, j).

GDF15 Suppresses Proliferation and Activation of B- and T-Cells in lpr Mice

Splenic mRNA analysis suggested a Th1-type interleukin-expression pattern. We observed significantly increased *Il-2,* which acts as a T-cell growth factor as well as elevated *Il23* expression, which promotes Th1/Th17 cell differentiation [28, 29]. Both *Il-4* and *Il-5* mRNA tended to be downregulated, but no significant differences were observed (Fig. 2a). Flow cytometric analysis of splenocytes revealed expansion of CD3+CD4+ and CD3+CD8+ T-cells. The percentage of activated

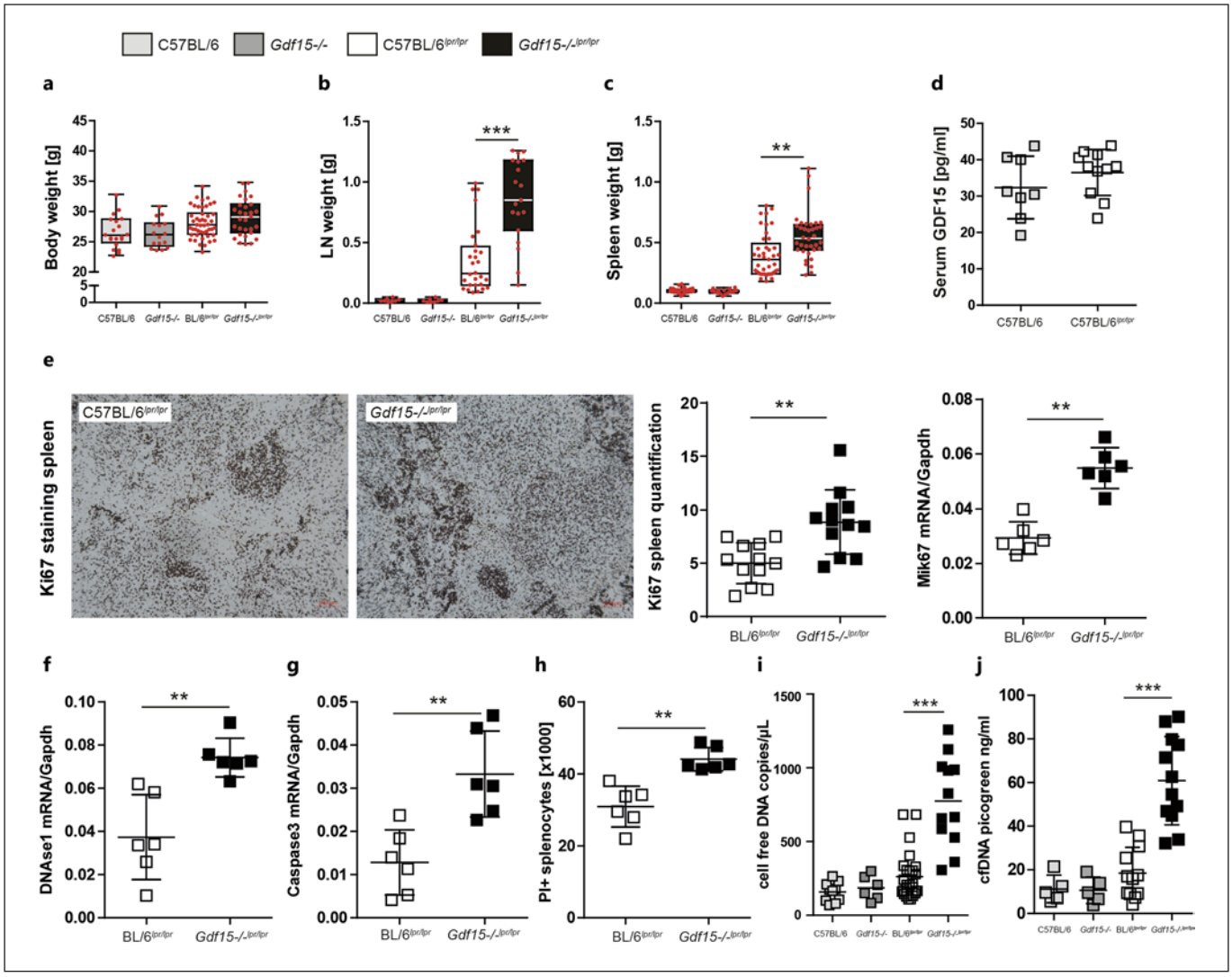

Fig. 1. GDF15 suppresses systemic lymphoproliferative disease in 6-month-old lupus-prone C57BL/6$^{lpr/lpr}$ mice. **a** 6-month-old C57BL/6 (n = 20), *Gdf15*–/– (n = 16), C57BL/6$^{lpr/lpr}$ (n = 49) and *Gdf15*–/–$^{lpr/lpr}$ (n = 30) female mice showed normal body weights. At 6 months of age female GDF15-deficient C57BL/6$^{lpr/lpr}$ mice showed increased cervical, axillar, and mesenteric lymph node- (**b**) as well as spleen-weights (**c**) compared with C57BL/6$^{lpr/lpr}$ or GDF15-deficient or intact C57BL/6, respectively (n = 8–41 as indicated in a figure). Data are presented as box-whiskers-plots, $^{**}p < 0.01$; $^{***}p < 0.001$. **d** C57BL/6 (n = 8) and C57BL/6$^{lpr/lpr}$ (n = 11) female mice were bled at age of 6 months to determine the serum levels of GDF15 protein. **e** Spleen sections of 6-month-old C57BL/6$^{lpr/lpr}$ (n = 12) and *Gdf15*–/–$^{lpr/lpr}$ (n = 12) female mice were stained with Ki67 proliferation marker (brown) and quantified (dot plot) using image software. RNA was isolated from spleens of 6 months old female *Gdf15*–/–$^{lpr/lpr}$ (n = 6) and control C57BL/6$^{lpr/lpr}$ (n = 6) mice for real-time PCR analysis. Data are expressed as means of the ratio of *Ki67* versus that of *GAPDH* mRNA. Data are presented as means ± SD, $^{**}p < 0.01$ versus control mice. **f**, **g** RNA was isolated from *Gdf15*–/–$^{lpr/lpr}$ (n = 6) and control C57BL/6$^{lpr/lpr}$ (n = 6) mice. Real-time PCR analysis represents *DNAse-I* and *Caspase-3* relative expression; $^{**}p < 0.01$ versus control mice. **h** PI+ splenocytes were quantified by flow cytometry ($^{**}p < 0.01$). Cell-free DNA was quantified in serum by real-time PCR (n = 6 per group) (**i**) and picogreen assay (**j**). Data are presented as means ± SD (**j**), $^{***}p < 0.001$ versus control mice (n = 6–26 per group as indicated in a figure).

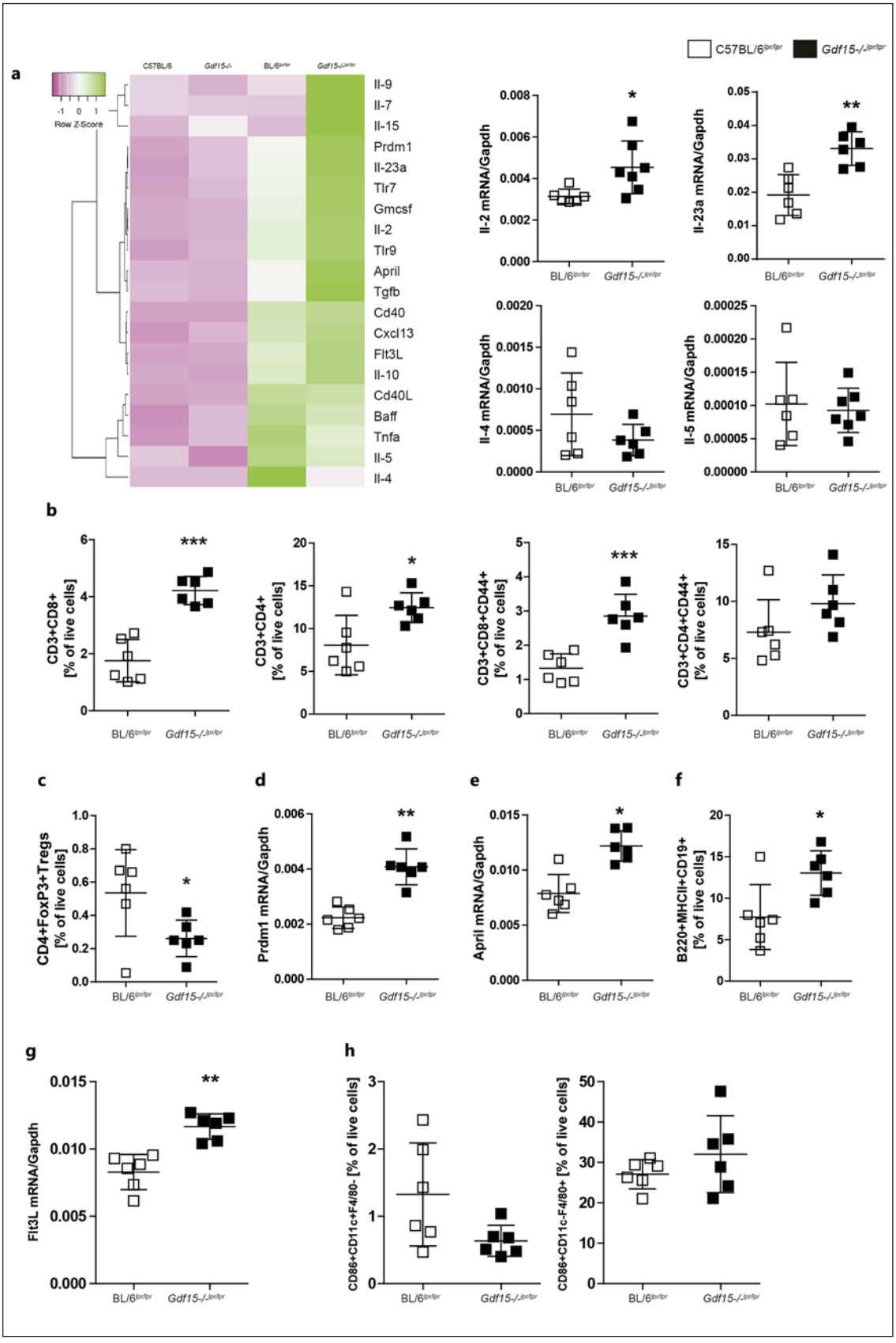

2

(For legend see next page.)

CD3+CD8+CD44+ cell subset was also significantly increased in *Gdf15*−/−$^{lpr/lpr}$ animals (Fig. 2b). Despite that, lower frequencies of CD4+FoxP3+ regulatory T cells were observed (Fig. 2c). This was associated, with upregulation of B-cell-differentiating transcripts, i.e., *Prdm-1* and *April* and increased frequencies of B220+ MHCII+ CD19+ B cells in spleens of *Gdf15*−/−$^{lpr/lpr}$ mice (Fig. 2d–f). Despite increased *Flt3l* levels, we found reduced CD11c+ dendritic cells frequency and similar levels of F4/80+ myeloid cells in spleens of *Gdf15*−/−$^{lpr/lpr}$ compared with C57BL/6$^{lpr/lpr}$ mice (Fig. 2g, h). Absolute cell counts of these cells can be retrieved from online supplementary Figure 1. Thus, GDF15 suppresses the proliferation and activation of T- and B- cells in the context of murine systemic autoimmunity.

GDF15 Suppresses Type I Interferon Signature, Autoantibody Production, and Renal Damage in lpr Mice

Next, we assessed female *Gdf15*−/−$^{lpr/lpr}$ mice for two hallmarks of lupus-like disease namely, type I interferon production and humoral autoimmunity. Whole spleen mRNA analysis revealed upregulation of type I and III interferon-dependent signaling pathways, i.e., increased *Ifit-1, Ifit-3, Zbp1, Ifnλ2, and Ifnλ3* expression (Fig. 3a, b). Moreover, classical Th1-cytokines, i.e., IFNγ, IL-12, and TNFα were increased in *Gdf15*−/−$^{lpr/lpr}$ mice (Fig. 3c). Despite lower frequencies of B220+ CD11c+ CD137+ "plasmacytoid dendritic" cells, GDF15-deficiency promoted increased serum levels of IFNα in autoimmune mice (Fig. 3d, e). We then assessed the splenic expression of plasma cell maturation repressor BLIMP-1 which drives

Fig. 2. GDF15 selectively controls the activation of T lymphocytes. **a** We presented the expression of relevant genes from spleens of 6-month-old C57BL/6, *Gdf15*−/−, C57BL/6$^{lpr/lpr}$, and *Gdf15*−/−$^{lpr/lpr}$ female mice (n = 5 per genotype) in form of a heatmap. The separation of autoimmunity patterns was based on average linkage hierarchical clustering. Dark pink colors on the heatmaps represent low expression values, whitish colors represent average values, and the green represents high values. The row *Z*-scores were used to ensure that the expression patterns are not overwhelmed by the expression values. Several genes that displayed different regulation between C57BL/6$^{lpr/lpr}$ (n = 6) and *Gdf15*−/−$^{lpr/lpr}$ (n = 7) genotypes in the preliminary experiment were selected for real-time RT-qPCR validation. **b** The percentage of (activated) T cells was assessed from spleens of 6-months old females by flow cytometry in *Gdf15*−/−$^{lpr/lpr}$ (n = 6) and control C57BL/6$^{lpr/lpr}$ (n = 6) mice. After dead cell exclusion (PI+) cells, CD3+CD4+CD8-(CD44+) and CD3+CD4−CD8+(CD44+) were gated according to online supplementary Figure 4. **c** The frequency of T regulatory cells in spleens was reduced in *Gdf15*−/−$^{lpr/lpr}$ (n = 6) compared to control (n = 6) mice. **d**, **e** The expression of Prdm1 and April in spleens from 6-month-old *Gdf15*−/−$^{lpr/lpr}$ (n = 6) and control C57BL/6$^{lpr/lpr}$ (n = 6) female mice. **f** Reports frequencies of spleen B220+ CD19+ MHCII+ B-cells (% of alive cells after PI dead cell exclusion as depicted in the online suppl. Fig. 4) in *Gdf15*−/−$^{lpr/lpr}$ (n = 6) versus C57BL/6$^{lpr/lpr}$ (n = 6) mice. **g** RNA was isolated from spleens of *Gdf15*−/−$^{lpr/lpr}$ (n = 6) and control C57BL/6$^{lpr/lpr}$ (n = 6) mice for real-time PCR analysis of Flt3L. **h** After exclusion of dead cells (PI) percentage of CD86+ CD11c+ F4/80- dendritic cells and CD86+ F4/80+ CD11c-macrophages were assessed from spleens of 6-month-old *Gdf15*−/−$^{lpr/lpr}$ (n = 6) and control C57BL/6$^{lpr/lpr}$ (n = 6) female mice by flow cytometry. Data represent means ± SD; *p < 0.05; **p < 0.01; ***p < 0.001.

Fig. 3. GDF15 suppresses type I interferon signature and autoantibody production in lupus-prone mice. **a** RNA was isolated from spleens of C57BL/6 (n = 5), *Gdf15*−/− (n = 6), *Gdf15*−/−$^{lpr/lpr}$ (n = 7), and control C57BL/6$^{lpr/lpr}$ (n = 6) female mice for real-time PCR analysis of pro-inflammatory and interferon signature genes *Ifit1* and *Ifit3*. **b** RNA was isolated from spleens of Gdf15−/−$^{lpr/lpr}$ (n = 7) and control C57BL/6$^{lpr/lpr}$ (n = 6) female type I and type III interferon signature genes. Data are presented as means ± SD, *p < 0.05; **p < 0.01 versus control mice. **c** C57BL/6 (n = 11–21), *Gdf15*−/− (n = 10–15), *Gdf15*−/−$^{lpr/lpr}$ (n = 10–30) and control C57BL/6$^{lpr/lpr}$ (n = 10–17) female mice were bled at month 6 to determine serum levels of IL-6, IL-12, IL-10, IFN-γ, MCP-1, and TNF-α; **p < 0.01; ***p < 0.001. **d** Furthermore, the levels of IFN-α were determined in serum (n = 6–14 per genotype). Data represent means ± SD; **p < 0.01. **e** Percentage of B220+ CD11c+ CD137+ spleen – pDCs were quantified in 6-month-old female mice (n = 6 per genotype) by flow cytometry. The graph presents the mean ± SD; *p < 0.05. **f** Spleen sections from C57BL/6 (n = 8), *Gdf15*−/− (n = 8), *Gdf15*−/−$^{lpr/lpr}$ (n = 8), and control C57BL/6$^{lpr/lpr}$ (n = 8) female mice were stained with antibodies against B220 and BLIMP1. The positive signal was quantified by PhotoShop Software (positive area per HPF). Data are presented as means ± SD, *p < 0.05; **p < 0.01 versus control mice. **g** Mature kappa-light chain+ CD138+ plasma cells were quantified in spleens of 6-month-old female mice (n = 9 per genotype) by flow cytometry. The histogram presents the mean ± SD, **p < 0.01 versus control mice. **h**, **i** C57BL/6 (n = 5–20), *Gdf15*−/− (n = 6–12), *Gdf15*−/−$^{lpr/lpr}$ (n = 8–19) and control C57BL/6$^{lpr/lpr}$ (n = 8–32) female mice were bled at month 6 to determine serum levels of immunoglobulins as well as (**i**) anti-dsDNA, anti-Smith, and anti-histones autoantibodies by ELISA. The lupus strain of mice with the severe phenotype (MRL$^{lpr/lpr}$; n = 4–5) was used as a positive control. The (n) number of animals is for every genotype per assay is indicated in a figure. The specificity of anti-dsDNA antibodies was confirmed by *Crithidiae luciliae* assay (data not shown). Data show means ± SD; *p < 0.05; **p < 0.01. HPF, high power field.

(For legend see next page.)

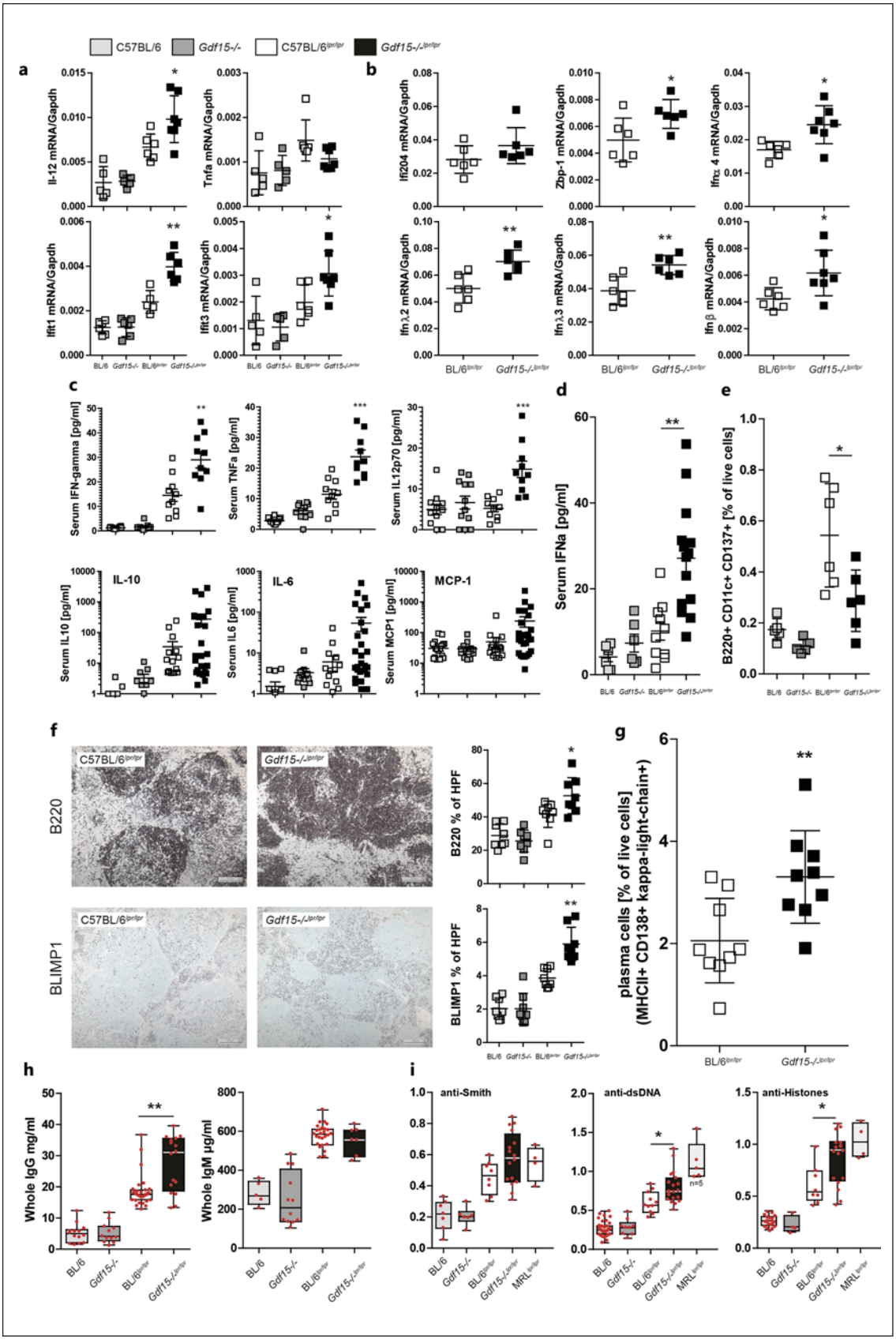
C57BL/6
Gdf15-/-
C57BL/6lpr/lpr
Gdf15-/-lpr/lpr
a
b
c
d
e
f
g
h
i
Il-12 mRNA/Gapdh
Tnfa mRNA/Gapdh
Ifit1 mRNA/Gapdh
Ifit3 mRNA/Gapdh
Ifi204 mRNA/Gapdh
Zbp-1 mRNA/Gapdh
Ifnα 4 mRNA/Gapdh
Ifnλ2 mRNA/Gapdh
Ifnλ3 mRNA/Gapdh
Ifnβ mRNA/Gapdh
Serum IFN-gamma [pg/ml]
Serum TNFa [pg/ml]
Serum IL12p70 [pg/ml]
Serum IL10 [pg/ml]
IL-10
Serum IL6 [pg/ml]
IL-6
Serum MCP1 [pg/ml]
MCP-1
Serum IFNa [pg/ml]
B220+ CD11c+ CD137+ [% of live cells]
B220
BLIMP1
B220 % of HPF
BLIMP1 % of HPF
plasma cells [% of live cells]
(MHCII+ CD138+ kappa-light-chain+)
Whole IgG mg/ml
Whole IgM µg/ml
anti-Smith
anti-dsDNA
anti-Histones
n=5
BL/6
Gdf15-/-
BL/6lpr/lpr
Gdf15-/-lpr/lpr
MRLlpr/lpr

3

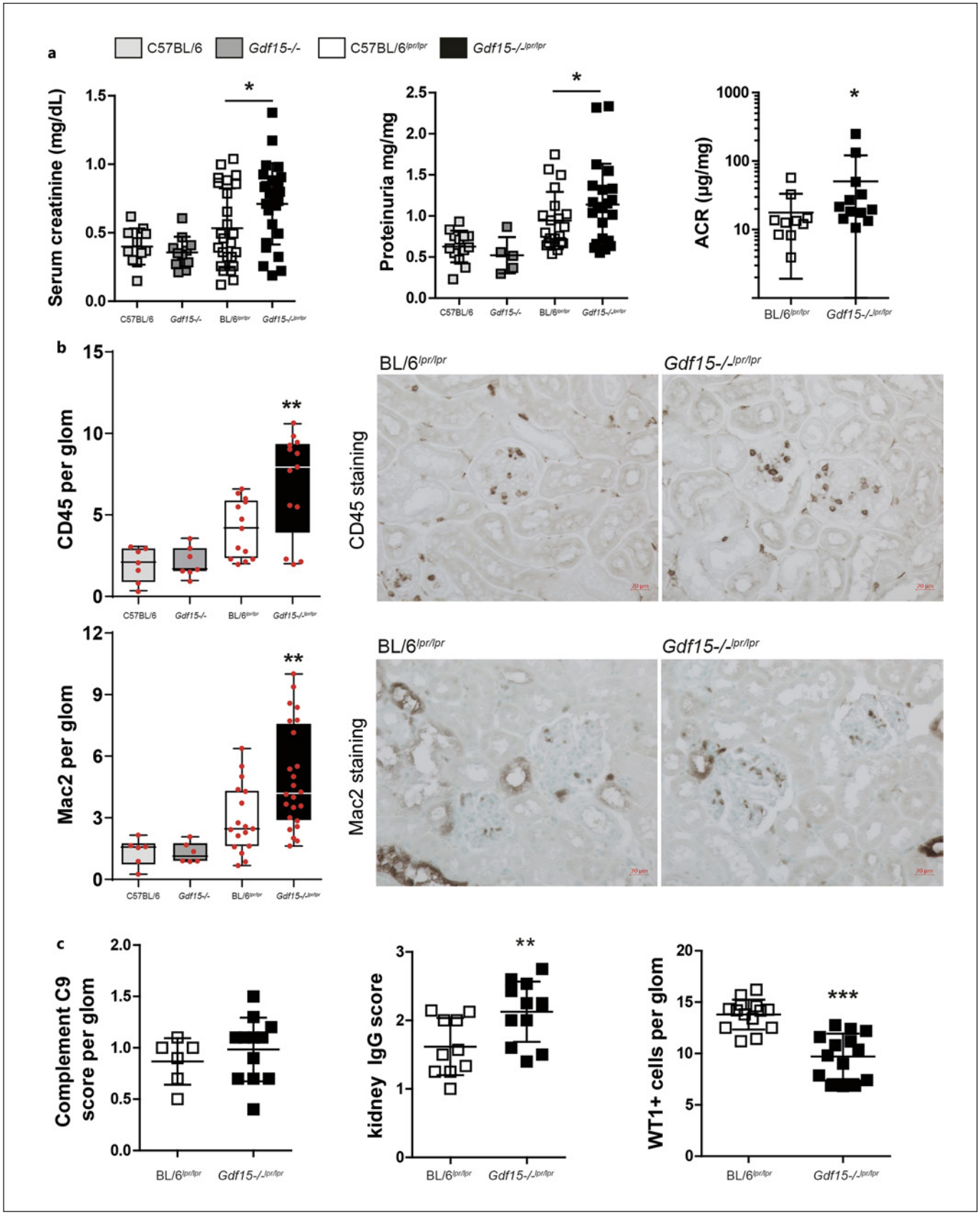

4

(For legend see next page.)

the terminal differentiation of B cells to plasma cells [30]. As expected we observed increased numbers of B220+ and BLIMP-1+ cells in *Gdf15–/–*$^{lpr/lpr}$ mice (Fig. 3f). Moreover, we detected more CD138+ kappa-light-chain+ plasma cells in spleens of *Gdf15–/–*$^{lpr/lpr}$ mice (Fig. 3g). This was associated with increased total IgM and IgG-serum levels (Fig. 3h; online suppl. Fig. 2) and higher levels of anti-ds-DNA- and anti-histone-autoantibodies in *Gdf15–/–*$^{lpr/lpr}$ animals, whereas anti-RNA/smith-directed auto-antibodies did not significantly differ (Fig. 3i).

These serologic features of SLE were accompanied by a mild renal phenotype in female *Gdf15–/–*$^{lpr/lpr}$ mice evidenced by increased serum creatinine levels, increased proteinuria and increased urinary albumin-creatinin-ratios (Fig. 4a). CD45-and MAC2-stainings revealed increased glomerular infiltration of leukocytes and predominantly macrophages in glomerular compartments (Fig. 4b). Despite similar complement activation, slightly increased glomerular IgG deposition and reduced counts of podocytes were found (Fig. 4c).

Taken together GDF15 accelerates the progression of autoimmune disease. It promotes enhanced interferon production, plasma cell maturation, autoantibody secretion, and results in aggravated nephritis without crescent formation.

GDF15 Negatively Regulates TLR-9 Dependent Proliferation and TLR-7 Dependent Serologic Features of Autoimmunity

Our data show that GDF15 deficiency alone was not sufficient to trigger autoimmunity at the age of 6 months. Yet, what could be the mechanism of how GDF15-deficiency aggravates autoimmunity in the lupus-prone C57BL/6$^{lpr/lpr}$ strain? *Gdf15–/–*$^{lpr/lpr}$ mice showed increased splenocyte cell death and increased cell-free DNA (Fig. 1h–j). Moreover, the increased production of serum inflammatory mediators like TNFα, IL-12, IFNγ, or IFNα (Fig. 3c, d) might be a possible mechanism. Still, no differences were detected in *Gdf15–/–* C57BL/6 versus C57BL/6 mice in these experiments (Fig. 3c, d). Comparable systemic corticosterone and aldosterone levels argue against a central immunomodulatory role of the GDF15-GFRAL-axis [10] (Fig. 5a).

Since endosomal TLRs, i.e., TLR-7 and -9 are involved in lupus pathogenesis, i.e., lymphocyte proliferation, as well as type-I interferon and anti-dsDNA-autoantibody production we tested splenic *Tlr7* and *Tlr9* expression and found the latter mildly increased in GDF15-deficient mice (Fig. 5b). Next, we stimulated macrophages of *Gdf15*-intact genotypes with the TLR-9 ligand CpG-DNA and assessed GDF15 levels from supernatants. Here, both wild-type C57BL/6 and lupus-prone C57BL/6$^{lpr/lpr}$ mice produced a significantly increased quantity of GDF15 (Fig. 5c). Splenocytes of GDF15-deficient mice showed enhanced proliferative responses after stimulation with CpG-DNA. This *Gdf15* dependent effect was apparent in C57BL/6 and lupus-prone C57BL/6$^{lpr/lpr}$ background (Fig. 5d). Further, stimulation of BMDMs with the TLR-9 and -7 ligands, CpG and Imiquimod resulted in increased expression of interferon dependent genes, i.e., type I interferon negative regulator *Ifi204*, *Ifit-1*, *and Ifit-3* in GDF15 deficient mice. This effect was observed for *Ifi204* after *CpG* and for *Ifit-1* and *Ifit-3* after Imiquimod exposure in both *lpr*- and non-*lpr* C57BL/6 strains (Fig. 5e). Consequently, *Gdf15* and *Gdf15–/–*$^{lpr/lpr}$ macrophages produced significantly more TNFα upon CpG stimulation. Stimulation of IFNγ-activated macrophages with CpG resulted in significantly increased IL-12 production (Fig. 5f). Of note, we performed similar experiments with cDCs and pDCs and did not find significant differences in response to CpG and Imiquimod stimulation with respect to interferon-dependent gene expression (online suppl. Fig. 3). Thus, GDF15 suppresses TLR-9 and -7 signaling-dependent pro-inflammatory and interferon-dependent gene expression in macrophages as well as TLR-9-dependent lymphocyte proliferation. As depicted in Figure 5f, combined stimulation of BMDMs with IFNγ+ CpG-DNA mimicking a lupus-like micro milieu resulted in significantly increased IL-12 and TNFα release in *Gdf15–/–* and *Gdf15–/–*$^{lpr/lpr}$ versus controls. Still, the induction of the interferon-dependent genes *Ifit-1* and *Ifit-3* was only enhanced upon activation of TLR-7 in *Gdf15–/–* animals versus controls (Fig. 5e). Taken together, these in vitro data demonstrate a negative regulatory role for GDF15 on TLR-9 and TLR-7 signaling.

Fig. 4. GDF15 reduces kidney injury in 6-month-old lupus-prone mice. **a** Kidney function parameters (serum creatinine, proteinuria and albumin/creatinine ratio) were measured in all groups of 6-month-old female mice (n = 10–25; the $n$is for every genotype per assay is indicated in a figure). Data are presented as means ± SD; *$p < 0.05$. **b** Kidney sections from C57BL/6 (n = 6–7), Gdf15–/– (n = 6–7), *Gdf15–/–*$^{lpr/lpr}$ (n = 14–24), and control C57BL/6$^{lpr/lpr}$ (n = 14–17) female mice were stained with antibodies against Mac2 and CD45, as well as (**c**) complement component 9 (C9) (n = 6 and n = 12), total IgG (n = 10 and n = 12), and WT1 (n = 14 and n = 14). The pathological changes were quantified by cell counting or by using a semiquantitative score. Data are shown as box-whiskers-plots or means ± SD; **$p < 0.01$, ***$p < 0.001$. n = number of animals is indicated in the figure.

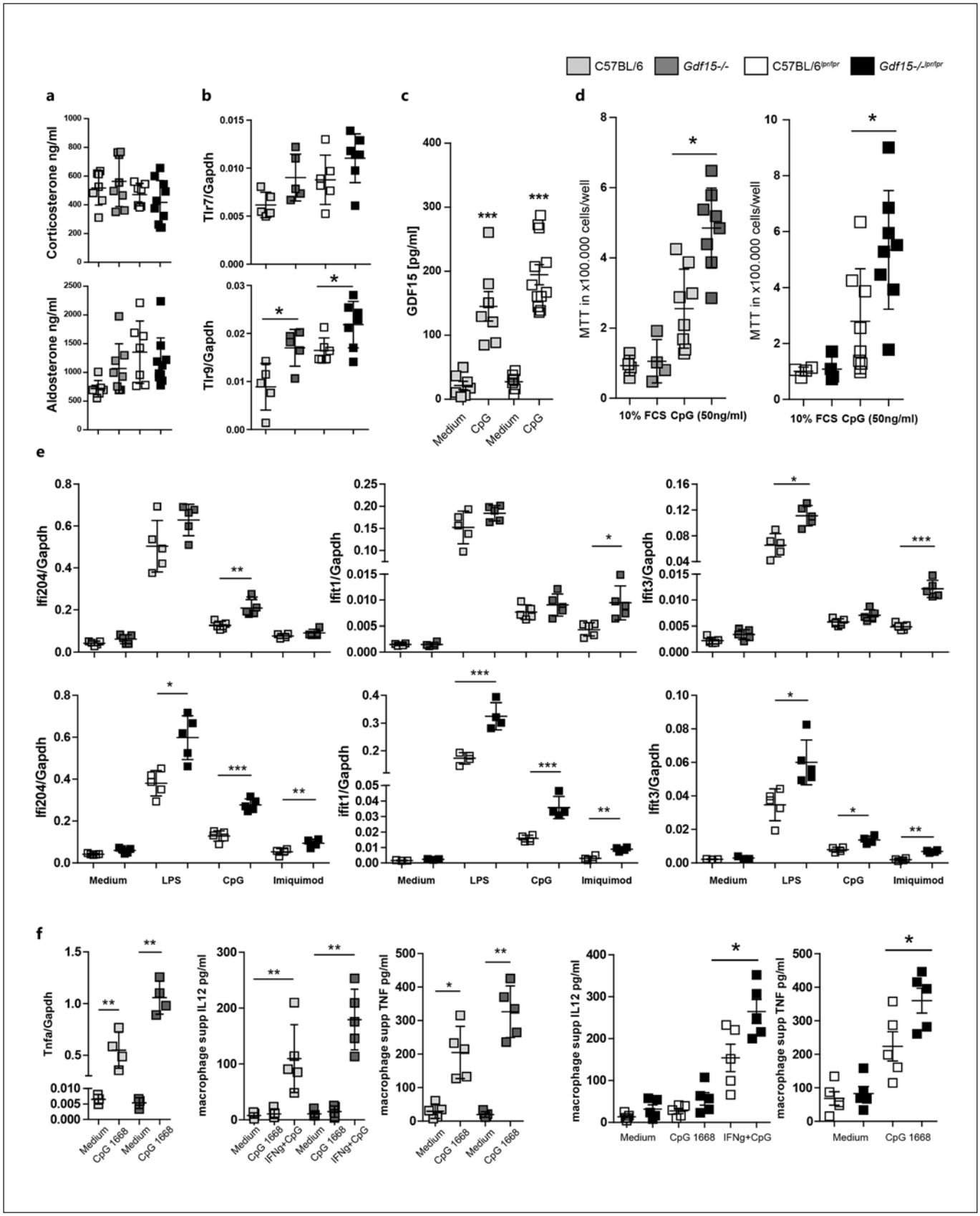

5

(For legend see next page.)

GDF15 Expression Is Downregulated in Human LN

Our data highlight the role of *Gdf15* in controlling serologic activity in murine SLE but does not investigate the relevance of GDF15 in human disease. Kidney involvement is the most common visceral organ manifestation in human SLE [2]. Therefore, we examined glomerular and tubular kidney tissue from patients with LN for abnormal expression of *GDF15* and interferon-dependent genes (i.e., *IFIT-1* and *IFIT-3*). Biopsy material from living kidney donors (LD) served as reference values. Kidney specimens affected from MCD or HTN served as "low-inflammatory" controls. In glomerular compartments, *GDF15* expression was downregulated in LN, as well as HTN and MCD specimens. Still, only in LN, we have found a concomitant strong upregulation of interferon-dependent gene- and *MKI67*- expression (Fig. 6a). In LN, whereas glomerulonephritis is regarded as a manifestation of systemic autoimmunity, tubulointerstitial inflammation is thought to reflect a prognostically relevant local inflammation-amplification-loop [31]. Interestingly, in tubular compartments, we observed the same pattern of downregulated *GDF15*, yet upregulated type I interferon-dependent gene expression (Fig. 6b). To assess whether *GDF15* mRNA levels were related to changes in interferon-dependent genes (i.e., IFIT-1 and IFIT-3) expression, we performed Spearman's correlation analysis among LN patients and healthy controls. We found a significant negative correlation between *GDF15* and tested interferon-dependent genes in glomerular (rho = −0.30 and −0.36, respectively, $p < 0.01$) compartments. This was even more pronounced in tubular compartments of LN kidneys (rho = −0.50 and −0.53; $p < 0.001$).

Discussion

We had hypothesized a negative-regulatory role for GDF15 in the pathogenesis of systemic autoimmunity, i.e., murine lupus-like disease. The presented data support this concept as GDF15 acted as a suppressor of lymphoproliferation, B- and T-cell expansion, autoreactive plasma-cell-maturation, and consequently anti-DNA-directed autoantibody generation in the C57BL/6$^{lpr/lpr}$ model. Moreover, we found, that GDF15 suppresses type I interferon signature in lupus-prone mice. Yet, consistent with our previous data on negative regulators of TLR-signaling [32–34], an additional factor creating an autoimmune-convenient environment was required before this immunoregulatory role of *Gdf15* came into play.

Both, type I interferon and anti-dsDNA-autoantibody production, are hallmarks of systemic lupus or lupus-like disease. The type I interferon signature has been causally linked to SLE pathogenesis via (a) genetic gain-of-function variants-associated risk for disease, (b) induction of SLE-like phenotypes in interferon treated cancer patients, and (c) correlation of type I interferons with antinuclear antibodies (ANA)-titers, disease activity, and nephritis in lupus patients [35]. Lastly, anifrolumab, an inhibitory human IgG1κ monoclonal antibody to type I interferon receptor subunit 1, showed promising results in the recent TULIP-2 trial performed in patients with active SLE [36]. *Gdf15*−/− in lupus-prone C57BL/6$^{lpr/lpr}$ mice significantly enhanced the serologic IFNα and IFNγ production and enforced an inflammatory systemic cytokine profile of increased systemic TNFα and IL-12p70 serum levels [37]. These data are consistent with previously published in

Fig. 5. GDF15 negatively regulates TLR-9 dependent inflammation and cell proliferation. **a** C57BL/6 ($n = 7$), *Gdf15*−/− ($n = 8$), *Gdf15*−/−$^{lpr/lpr}$ ($n = 10$) and control C57BL/6$^{lpr/lpr}$ ($n = 7$) female mice were bled at month 6 to determine serum levels of corticosterone and aldosterone. Data represent means ± SD. **b** Expression levels of *Tlr7* and *Tlr-9* in spleens of 6-month-old C57BL/6 ($n = 5$), *Gdf15*−/− ($n = 5$), *Gdf15*−/−$^{lpr/lpr}$ ($n = 6$), and control C57BL/6$^{lpr/lpr}$ ($n = 6$) females were quantified by real-time PCR. Data are shown as means ± SD of the ratio of the specific mRNA versus that of *GAPDH* mRNA, $^{*}p < 0.05$. **c** The production of GDF15 was quantified in supernatants of BM derived macrophage isolated from C57BL/6 ($n = 7$) and C57BL/6$^{lpr/lpr}$ ($n = 12$) mice by ELISA 24 h upon CpG 1668 (100 ng/mL) stimulation. Data represent means ± SD; $^{***}p < 0.001$. **d** The proliferative activity of spleen lymphocytes isolated from 8-weeks old mice, stimulated with 10% FCS ($n = 4$) or CpG ($n = 8$) was evaluated by MTT assay 72 h upon CpG 1668 (50 ng/mL). The graphs represent a representative experiment (from three independent experiments) performed in a single run; presented as mean ± SD; $^{*}p < 0.05$. **e** Expression analysis of preselected interferon type I dependent genes in BM-derived macrophages isolated from all four strains of mice and stimulated with LPS (10 ng/mL), CpG 1668 (100 ng/mL), and Imiquimod (1 μg/mL); $n = 5$ per each group and genotype. The expression of selected genes was determined in BM-derived macrophages 4 h post-stimulation. The graphs represent a representative experiment (from three independent experiments) performed in a single run. Data represent means ± SD; $^{*}p < 0.05$; $^{**}p < 0.01$, $^{***}p < 0.001$. **f** The differences in *TNFα* expression ($n = 4$ per genotype and stimulation) and IL12 and TNFα production upon CpG 1668 (100 ng/mL) stimulation (or costimulation with 20 ng/mL of IFNγ) in BM-derived macrophages from C57BL/6, *Gdf15*−/− as well as *Gdf15*−/−$^{lpr/lpr}$ and control C57BL/6$^{lpr/lpr}$ mice were evaluated with qPCR (4 h) and ELISA (24 h). The biological replicates of $n = 5$ per group were used. Data represent means ± SD; $^{*}p < 0.05$; $^{**}p < 0.01$. The graphs represent a representative experiment (from three independent experiments) performed in a single run.

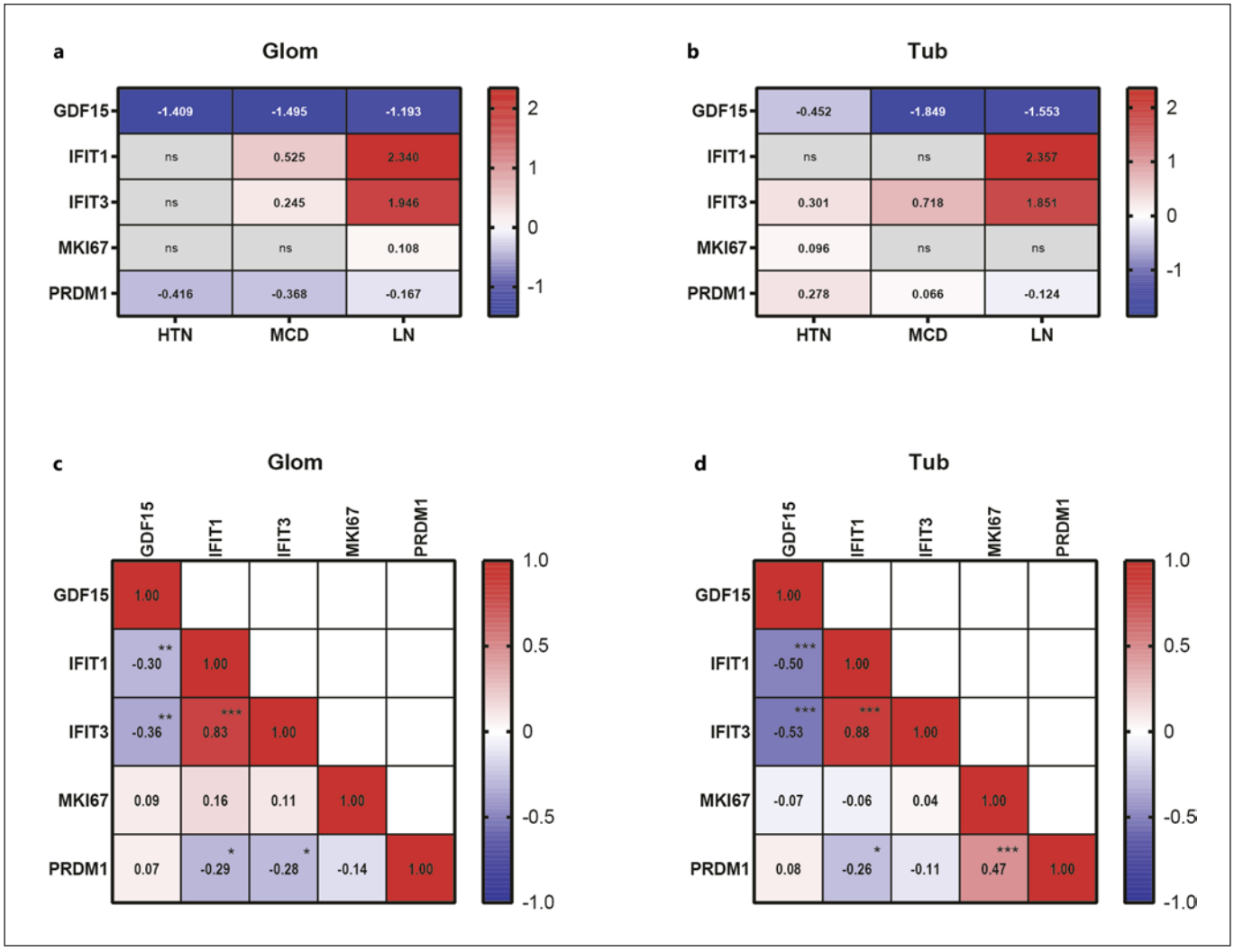

Fig. 6. GDF15 expression in human LN. Gene expression analysis of *GDF15, IFIT1, IFIT3, MKI67*, and *PRDM1* genes in glomerular (**a**) and tubular (**b**) compartment of manually microdissected kidney biopsies from patients with HTN (Glom: $n = 15$; Tub: $n = 21$), MCD (Glom: $n = 14$; Tub: $n = 15$), and LN (Glom: $n = 32$; Tub: $n = 32$). Pretransplantation kidney biopsies from LDs (Glom: $n = 42$, Tub: $n = 42$) were used as control renal tissue. Values are expressed as a log2-fold change compared to controls (LD). All represented genes are significantly changed ($p < 0.05$), except when indicated n.s. Spearman correlation matrix for each gene-gene correlation in glomeruli (**c**) and tubulointerstitium (**d**) of patients ($n = 32$) with LN and ($n = 42$) controls (LDs). Shown are the Spearman correlation coefficients. A p value below 0.05 was considered to be statistically significant ($^*p < 0.05$, $^{**}p < 0.01$, $^{***}p < 0.001$). n.s., not significant.

vivo data on diabetic mice, where GDF15 was shown to inhibit pro-inflammatory macrophage polarization [17].

Our data highlight TLR-7/-9 hyperresponsiveness as possible mechanisms of the exaggerated type I signature in GDF15-deficient C57BL/6$^{lpr/lpr}$ mice. Although, plasmacytoid dendritic cells were considered the classical interferon producers in SLE, in the meantime macrophages have also been implicated in this process [38–41]. In *Gdf15*−/− C57BL/6$^{lpr/lpr}$ mice, the frequency of B220+ CD11c+ CD137+ dendritic cells was not enhanced in spleens and ex vivo TLR-7/-9 hyperresponsiveness was detected in BMDMs but not BMDCs, consistent with an important role of macrophages in type I IFN production.

Apart from exaggerated serologic autoimmune activity, GDF15-deficiency was associated with a mild nephritic phenotype in mice as evidenced by increased glomerular IgG deposits, mild hypercellularity, reduced podocytes numbers, and increased albumin creatinine ra-

tios. However, we did not observe full-blown crescentic LN. One might argue that 6 months of observation might have been too short to observe full-blown nephritis. Yet, similar experiments by our group investigating other negative regulators of innate immunity, e.g., SIGIRR or the NLRP3 inflammasome components revealed stronger histologic evidence of renal injury or bronchiolitis/pneumonitis at the same age [32, 42].

In acute murine anti-GBM nephritis in C57BL/6 mice, GDF15-deficiency promoted CXCL10/CXCR3-dependent T-cell infiltration and crescent formation [32]. In addition, Liu et al. [43] recently demonstrated that increased GDF15 level in tubular epithelial cells upon ischemia-reperfusion injury prevented post-ischemia inflammation and injury. Although GDF15 has a similar renal protective effect in all these models, its effect size varies between acute versus chronic inflammation.

The question remains of how GDF15 flips the immunoregulatory switch in murine lupus-like autoimmunity. Up to recently, only the CNS receptor GFRAL had been a confirmed interaction partner of GDF15 [9]. Luan et al. [10] recently proposed a model in which GDF15 acts as a central mediator of inflammatory tissue tolerance in sepsis via a central regulatory mechanism controlling hepatic lipid export in a GDF15-GFRAL-sympathetic-axis-dependent manner. Yet, C57BL/6 and C57BL/$6^{lpr/lpr}$ mice showed comparable systemic levels of GDF15 at the age of 6 months when autoantibodies and lymphoproliferation were already established and systemic corticoid hormone levels were comparable amongst *Gdf15*−/− and control mice. Therefore, a central regulator mechanism seems unlikely in our model.

Instead, it was recently shown that GDF15 suppresses anti-(HCC)-tumor immunity via CD48 engagement on Tregs [14]. In fact, *Gdf15*−/− C57BL/$6^{lpr/lpr}$ mice displayed reduced peripheral Treg counts. Reduced Tregs however are a frequent finding in an active murine and human SLE [44]. Scurfy mice, which display a missense mutation in the transcription factor Foxp3 and are deficient in Tregs, develop early-onset hyperinflammation, autoantibodies, and lymphoproliferation [45]. Thus, reduced regulatory T-cell activity, which we were unable to assess in vivo, could explain some aspects of the observed phenotype but falls short of explaining the prominent type I interferon/interferon-alpha production in our mice [45].

Instead, we demonstrate a direct immunosuppressive effect of *Gdf15* on macrophage TLR7 and TLR-9-signaling in C57BL/6 and C57BL/$6^{lpr/lpr}$ mice in vitro. Similarly, others have demonstrated that GDF-15 suppresses macrophage inflammatory cytokine release and T-cell activation in alcohol-induced chronic liver injury in mice [46]. While most phenotypic alterations in *Gdf15*−/− C57BL/$6^{lpr/lpr}$ mice, e.g., increased cfDNA, type I interferon- and anti-dsDNA-autoantibody production were absent in *Gdf15*−/− C57BL/6 mice, TLR-9-dependent-splenocyte proliferation, TLR-9-dependent-macrophage-cytokine secretion, and TLR7 dependent *Ifit-1* and -3 expression were already apparent in *Gdf15*−/− C57BL/6 mice. In accordance, type I interferon signature and anti-dsDNA autoantibody production is closely tied to aberrant signaling of innate DNA-sensors in the early pathogenesis of SLE [47, 48]. Immune complexes are known ligands of TLR-7 and -9 and inducers of type I interferon in SLE macrophages [49].

Targeting TLR-7 with monoclonal antibodies was shown to reduce circulating monocytes and ameliorate LN in NZBWF1 mice [50]. Similarly, overexpression of TLR-7 aggravates type I interferon production, anti-RNA autoantibody secretion and nephritis in mice [51]. TLR-9-signaling on the other hand is relevant for anti-DNA autoantibody production but also protects against LN in lpr mice. We therefore consider both, increased TLR-9- and TLR-7-signaling, to be relevant for the immunologic features of *Gdf15*−/− C57BL/$6^{lpr/lpr}$ mice: autoantibodies and type I interferons (TLR-7 and TLR-9) versus LN (TLR-7) [52]. Clearly, this remains speculative, since the combined deletion of TLR-7/9 and GDF15 would be necessary to prove these considerations.

Our study has several limitations. Since we were unable to observe full-blown nephritis and mortality of *Gdf15*−/− C57BL/$6^{lpr/lpr}$ before the experiment was terminated. In addition, in vivo relevance of the proposed GDF15/TLR-inhibitory mechanism needs to be further investigated and requires a strategy involving combined knock out of multiple genes encoding *Tlr7*, *Tlr9*, and *Gdf15*.

Taken together, we demonstrate that GDF15 displays a disease-modifying effect in lupus-like autoimmunity. Thus, GDF15 suppresses lymphoproliferation, type I interferon-, and anti-DNA-autoantibody production in autoimmune-prone mice. Human data further indicates its involvement in human LN.

Acknowledgments

We thank all participating centers of the European Renal cDNA Bank – Kröner-Fresenius biopsy bank (ERCB-KFB) and their patients for their cooperation. Active members at the time of the study see [53].

Statement of Ethics

This study was carried out following the principles of the Directive 2010/63/EU on the Protection of Animals Used for Scientific Purpose and with approval by the local government authorities (ROB Az 55.2-1-54-2531-11-10). The study follows the ARRIVE guidelines. Human kidney biopsy specimens and Affymetrix microarray expression data were procured within the framework of the European Renal cDNA Bank-Kröner-Fresenius Biopsy Bank. Biopsies were obtained from patients after informed consent and with the approval of the local Ethics Committees (the Ethics Committee Reference Number #250-16 [Ethics Committee of medical faculty at LMU Munich]). Written informed consent was obtained from the patients.

Conflict of Interest Statement

The authors have no conflicts of interest.

Funding Sources

The study was funded by the Deutsche Forschungsgemeinschaft (LE2621/6-1) and National Science Center, Poland Grants 2016/23/B/NZ6/00086 to ML. The ERCB-KFB was supported by the Else Kröner-Fresenius Foundation.

Author Contributions

Georg Lorenz and Maciej Lech performed experiments and data analysis, designed the study, and wrote the manuscript. Andrea Ribeiro, Ekatharina von Rauchhaupt, Vivian Würf, Twinkle Vohra, and Maja Lindenmeyer performed experiments and data analysis. Hans-Joachim Anders, Christoph Schmaderer, Clemens D. Cohen, and Maja Lindenmeyer carefully read and improved the manuscript and were involved in data interpretation.

Data Availability Statement

Published gene expression profiles (Affymetrix GeneChip Human Genome U133A and U133 Plus2.0 Arrays; GSE99340, GSE32591, GSE35489, GSE37463) used in this study.

References

1 Kaul A, Gordon C, Crow MK, Touma Z, Urowitz MB, van Vollenhoven R, et al. Systemic lupus erythematosus. Nat Rev Dis Primers. 2016 Jun 16;2:16039.
2 Anders HJ, Saxena R, Zhao MH, Parodis I, Salmon JE, Mohan C. Lupus nephritis. Nat Rev Dis Primers. 2020 Jan 23;6(1):7.
3 Bootcov MR, Bauskin AR, Valenzuela SM, Moore AG, Bansal M, He XY, et al. MIC-1, a novel macrophage inhibitory cytokine, is a divergent member of the TGF-beta superfamily. Proc Natl Acad Sci U S A. 1997 Oct 14;94(21):11514–9.
4 Breit SN, Tsai VW, Brown DA. Targeting obesity and cachexia: identification of the GFRAL receptor-MIC-1/GDF15 pathway. Trends Mol Med. 2017 Dec;23(12):1065–7.
5 McPherron AC, Lee SJ. The transforming growth factor β superfamily. In: Leroith D, Bondy C, editors. Growth factors and cytokines in health and disease. JAI; 1996. p. 357–93.
6 Böttner M, Laaff M, Schechinger B, Rappold G, Unsicker K, Suter-Crazzolara C. Characterization of the rat, mouse, and human genes of growth/differentiation factor-15/macrophage inhibiting cytokine-1 (GDF-15/MIC-1). Gene. 1999 Sep 3;237(1):105–11.
7 Shull MM, Ormsby I, Kier AB, Pawlowski S, Diebold RJ, Yin M, et al. Targeted disruption of the mouse transforming growth factor-β1 gene results in multifocal inflammatory disease. Nature. 1992 Oct 1;359(6397):693–9.
8 Kulkarni AB, Huh CG, Becker D, Geiser A, Lyght M, Flanders KC, et al. Transforming growth factor beta 1 null mutation in mice causes excessive inflammatory response and early death. Proc Natl Acad Sci U S A. 1993 Jan 15;90(2):770–4.
9 Wischhusen J, Melero I, Fridman WH. Growth/differentiation factor-15 (GDF-15): from biomarker to novel targetable immune checkpoint. Front Immunol. 2020;11:951.
10 Luan HH, Wang A, Hilliard BK, Carvalho F, Rosen CE, Ahasic AM, et al. GDF15 is an inflammation-induced central mediator of tissue tolerance. Cell. 2019 Aug 22;178(5):1231–44.e11.
11 Kempf T, Eden M, Strelau J, Naguib M, Willenbockel C, Tongers J, et al. The transforming growth factor-beta superfamily member growth-differentiation factor-15 protects the heart from ischemia/reperfusion injury. Circ Res. 2006 Feb 17;98(3):351–60.
12 Kempf T, Zarbock A, Widera C, Butz S, Stadtmann A, Rossaint J, et al. GDF-15 is an inhibitor of leukocyte integrin activation required for survival after myocardial infarction in mice. Nat Med. 2011 May;17(5):581–8.
13 Moschovaki-Filippidou F, Steiger S, Lorenz G, Schmaderer C, Ribeiro A, von Rauchhaupt E, et al. Growth differentiation factor 15 ameliorates anti-glomerular basement membrane glomerulonephritis in mice. Int J Mol Sci. 2020 Sep 23;21(19):6978.
14 Wang Z, He L, Li W, Xu C, Zhang J, Wang D, et al. GDF15 induces immunosuppression via CD48 on regulatory T cells in hepatocellular carcinoma. J Immunother Cancer. 2021 Sep;9(9):e002787.
15 Shokrgozar N, Amirian N, Ranjbaran R, Bazrafshan A, Sharifzadeh S. Evaluation of regulatory T cells frequency and FoxP3/GDF-15 gene expression in β-thalassemia major patients with and without alloantibody; correlation with serum ferritin and folate levels. Ann Hematol. 2020 Mar;99(3):421–9.
16 Zhou Z, Li W, Song Y, Wang L, Zhang K, Yang J, et al. Growth differentiation factor-15 suppresses maturation and function of dendritic cells and inhibits tumor-specific immune response. PLoS One. 2013;8(11):e78618.
17 Jung SB, Choi MJ, Ryu D, Yi HS, Lee SE, Chang JY, et al. Reduced oxidative capacity in macrophages results in systemic insulin resistance. Nat Commun. 2018 Apr 19;9(1):1551.
18 Esalatmanesh K, Fayyazi H, Esalatmanesh R, Khabbazi A. The association between serum levels of growth differentiation factor-15 and rheumatoid arthritis activity. Int J Clin Pract. 2020 Sep;74(9):e13564.
19 Nakayasu ES, Syed F, Tersey SA, Gritsenko MA, Mitchell HD, Chan CY, et al. Comprehensive proteomics analysis of stressed human islets identifies gdf15 as a target for type 1 diabetes intervention. Cell Metab. 2020 Feb 4;31(2):363–74.e6.

20 Yan C, Yu L, Zhang XL, Shang JJ, Ren J, Fan J, et al. Cytokine profiling in Chinese SLE patients: correlations with renal dysfunction. J Immunol Res. 2020;2020:8146502.
21 Chavele KM, Ehrenstein MR. Regulatory T-cells in systemic lupus erythematosus and rheumatoid arthritis. FEBS Lett. 2011 Dec 1; 585(23):3603–10.
22 Ma WT, Gao F, Gu K, Chen DK. The role of monocytes and macrophages in autoimmune diseases: a comprehensive review. Front Immunol. 2019;10:1140.
23 Hsiao EC, Koniaris LG, Zimmers-Koniaris T, Sebald SM, Huynh TV, Lee SJ. Characterization of growth-differentiation factor 15, a transforming growth factor beta superfamily member induced following liver injury. Mol Cell Biol. 2000 May;20(10):3742–51.
24 Penzkofer T, Jäger M, Figlerowicz M, Badge R, Mundlos S, Robinson PN, et al. L1Base 2: more retrotransposition-active LINE-1s, more mammalian genomes. Nucleic Acids Res. 2017 Jan 4;45(D1):D68–d73.
25 Cohen CD, Gröne HJ, Gröne EF, Nelson PJ, Schlöndorff D, Kretzler M. Laser microdissection and gene expression analysis on formaldehyde-fixed archival tissue. Kidney Int. 2002;61(1):125–32.
26 Cohen CD, Klingenhoff A, Boucherot A, Nitsche A, Henger A, Brunner B, et al. Comparative promoter analysis allows de novo identification of specialized cell junction-associated proteins. Proc Natl Acad Sci U S A. 2006 Apr 11;103(15):5682–7.
27 Tusher VG, Tibshirani R, Chu G. Significance analysis of microarrays applied to the ionizing radiation response. Proc Natl Acad Sci U S A. 2001;98(9):5116–21.
28 Krausgruber T, Schiering C, Adelmann K, Harrison OJ, Chomka A, Pearson C, et al. T-bet is a key modulator of IL-23-driven pathogenic CD4(+) T cell responses in the intestine. Nat Commun. 2016 May 19;7:11627.
29 Ross SH, Cantrell DA. Signaling and function of interleukin-2 in T lymphocytes. Annu Rev Immunol. 2018 Apr 26;36:411–33.
30 Shaffer AL, Lin KI, Kuo TC, Yu X, Hurt EM, Rosenwald A, et al. Blimp-1 orchestrates plasma cell differentiation by extinguishing the mature B cell gene expression program. Immunity. 2002 Jul;17(1):51–62.
31 Clark MR, Trotter K, Chang A. The pathogenesis and therapeutic implications of tubulointerstitial inflammation in human lupus nephritis. Semin Nephrol. 2015;35(5):455–64.
32 Lech M, Kulkarni OP, Pfeiffer S, Savarese E, Krug A, Garlanda C, et al. Tir8/Sigirr prevents murine lupus by suppressing the immunostimulatory effects of lupus autoantigens. J Exp Med. 2008 Aug 4;205(8):1879–88.
33 Lech M, Kantner C, Kulkarni OP, Ryu M, Vlasova E, Heesemann J, et al. Interleukin-1 receptor-associated kinase-M suppresses systemic lupus erythematosus. Ann Rheum Dis. 2011 Dec;70(12):2207–17.
34 Lech M, Weidenbusch M, Kulkarni OP, Ryu M, Darisipudi MN, Susanti HE, et al. IRF4 deficiency abrogates lupus nephritis despite enhancing systemic cytokine production. J Am Soc Nephrol. 2011 Aug;22(8):1443–52.
35 Postal M, Vivaldo JF, Fernandez-Ruiz R, Paredes JL, Appenzeller S, Niewold TB. Type I interferon in the pathogenesis of systemic lupus erythematosus. Curr Opin Immunol. 2020 Dec;67:87–94.
36 Morand EF, Furie R, Tanaka Y, Bruce IN, Askanase AD, Richez C, et al. Trial of Anifrolumab in active systemic lupus erythematosus. N Engl J Med. 2020 Jan 16;382(3):211–21.
37 Martinez FO, Gordon S. The M1 and M2 paradigm of macrophage activation: time for reassessment. F1000Prime Rep. 2014;6:13.
38 Gilliet M, Cao W, Liu YJ. Plasmacytoid dendritic cells: sensing nucleic acids in viral infection and autoimmune diseases. Nat Rev Immunol. 2008 Aug;8(8):594–606.
39 Hoss A, Zwarthoff EC, Zawatzky R. Differential expression of interferon alpha and beta induced with Newcastle disease virus in mouse macrophage cultures. J Gen Virol. 1989 Mar;70(Pt 3):575–89.
40 Ratnam NM, Peterson JM, Talbert EE, Ladner KJ, Rajasekera PV, Schmidt CR, et al. NF-κB regulates GDF-15 to suppress macrophage surveillance during early tumor development. J Clin Invest. 2017 Oct 2;127(10):3796–809.
41 Ali S, Mann-Nüttel R, Schulze A, Richter L, Alferink J, Scheu S. Sources of type I interferons in infectious immunity: plasmacytoid dendritic cells not always in the driver's seat. Front Immunol. 2019;10:778.
42 Lech M, Lorenz G, Kulkarni OP, Grosser MO, Stigrot N, Darisipudi MN, et al. NLRP3 and ASC suppress lupus-like autoimmunity by driving the immunosuppressive effects of TGF-beta receptor signalling. Ann Rheum Dis. 2015 Dec;74(12):2224–35.
43 Liu J, Kumar S, Heinzel A, Gao M, Guo J, Alvarado GF, et al. Renoprotective and immunomodulatory effects of GDF15 following AKI invoked by ischemia-reperfusion injury. J Am Soc Nephrol. 2020;31(4):701–15.
44 Ohl K, Tenbrock K. Regulatory T cells in systemic lupus erythematosus. Eur J Immunol. 2015 Feb 1;45(2):344–55.
45 Brunkow ME, Jeffery EW, Hjerrild KA, Paeper B, Clark LB, Yasayko SA, et al. Disruption of a new forkhead/winged-helix protein, scurfin, results in the fatal lymphoproliferative disorder of the scurfy mouse. Nat Genet. 2001 Jan;27(1):68–73.
46 Chung HK, Kim JT, Kim HW, Kwon M, Kim SY, Shong M, et al. GDF15 deficiency exacerbates chronic alcohol- and carbon tetrachloride-induced liver injury. Sci Rep. 2017 Dec 8; 7(1):17238.
47 Shrivastav M, Niewold TB. Nucleic acid sensors and type I interferon production in systemic lupus erythematosus. Front Immunol. 2013 Oct 7;4:319.
48 Lorenz G, Lech M, Anders HJ. Toll-like receptor activation in the pathogenesis of lupus nephritis. Clin Immunol. 2017 Dec;185:86–94.
49 Henault J, Martinez J, Riggs JM, Tian J, Mehta P, Clarke L, et al. Noncanonical autophagy is required for type I interferon secretion in response to DNA-immune complexes. Immunity. 2012 Dec 14;37(6):986–97.
50 Murakami Y, Fukui R, Tanaka R, Motoi Y, Kanno A, Sato R, et al. Anti-TLR7 antibody protects against lupus nephritis in NZBWF1 mice by targeting B cells and patrolling monocytes. Front Immunol. 2021;12:777197.
51 Myhre PL, Prebensen C, Strand H, Røysland R, Jonassen CM, Rangberg A, et al. Growth differentiation factor 15 provides prognostic information superior to established cardiovascular and inflammatory biomarkers in unselected patients hospitalized with COVID-19. Circulation. 2020 Dec;142(22): 2128–37.
52 Christensen SR, Shupe J, Nickerson K, Kashgarian M, Flavell RA, Shlomchik MJ. Toll-like receptor 7 and TLR9 dictate autoantibody specificity and have opposing inflammatory and regulatory roles in a murine model of lupus. Immunity. 2006 Sep;25(3):417–28.
53 Shved N, Warsow G, Eichinger F, Hoogewijs D, Brandt S, Wild P, et al. Transcriptome-based network analysis reveals renal cell type-specific dysregulation of hypoxia-associated transcripts. Sci Rep. 2017;7(1):8576–6.